European Cells and Materials Vol. 24 2012 (pages 60-73) DOI: 10.22203/eCM.v024a05 ISSN 1473-2262

SPECTROSCOPY IN THE ANALYSIS OF BACTERIAL AND EUKARYOTIC CELL FOOTPRINTS ON IMPLANT SURFACES

E. Kaivosoja[1,2], S. Virtanen[3], R. Rautemaa[4,5,6,7], R. Lappalainen[8] and Y.T. Konttinen[1,9,10,*]

[1]Department of Medicine, Institute of Clinical Medicine, Helsinki University Central Hospital, Finland
[2]Department of Electronics, School of Electrical Engineering, Aalto University, Finland [3] Department of Materials Science and Engineering, Chair for Surface Science and Corrosion, Friedrich-Alexander-University of Erlangen-Nüremberg, Germany
[4]Department of Bacteriology and Immunology, Haartman Institute, University of Helsinki, Finland
[5]Department of Oral Medicine, Institute of Dentistry, University of Helsinki [6]Department of Oral and Maxillofacial Diseases, Helsinki University Central Hospital, Finland
[7]The University of Manchester, Manchester Academic Health Science Centre, School of Translational Medicine and University Hospital of South Manchester, UK
[8]Department of Applied Physics, Kuopio Campus, University of Eastern Finland, Kuopio, Finland
[9]ORTON Orthopaedic Hospital of the ORTON Foundation, Helsinki, Finland
[10]COXA Hospital for Joint Replacement, Tampere, Finland

Abstract

We tested the suitability of two spectroscopic methods, x-ray photoelectron spectroscopy (XPS) and time of flight secondary ion mass spectrometry (ToF-SIMS), in the recognition of bacterial and eukaryotic cell footprints on implant surfaces. Human mesenchymal stem cells (MSCs) and *Staphylococcus aureus* were cultured on sample surfaces and detached using trypsin. Scanning electron microscopy confirmed that the processed surfaces did not contain any human or microbial cells. The footprints were then analysed using XPS and ToF-SIMS. XPS results showed no significant differences between the footprints, but principal component analysis of the ToF-SIMS data enabled clear separation of MSC-footprints from the *S. aureus* and co-culture footprints ($p < 0.03$). ToF-SIMS also demonstrated 'race for the surface' between proteins, which suggest surface charge (zeta-potential) dependent protein adsorption. ToF-SIMS differentiated eukaryotic and bacterial footprints and has potential for *post-hoc* detection of implant-related infections based on the typical ToF-SIMS spectra.

Keywords: Bacterial infection; time of flight secondary ion mass spectrometry; x-ray photoelectron spectroscopy.

*Address for correspondence:
Y.T. Konttinen
PO Box 70
00029 HUS, Finland

FAX Number: +358-9-191 25218
E-mail: yrjo.konttinen@helsinki.fi

Introduction

Bacterial infections remain an important cause of failure of many types of implants (Darouiche, 2001; Darouiche, 2004). Infected abiotic and immune-compromised implant surfaces and materials act as bacterial growth substrates and reservoirs, impairing implant function, propagating local spreading of the infection into surrounding tissues and haematogenic "metastatic" infections into distant sites. Recognition of the colonisation of the implant surface by bacteria remains an important clinical and academic issue.

Reliable recognition of bacterial infection in implant-related infections is challenging. The classical diagnostic method is bacterial culture of the periprostetic tissues and fluids. However, recognition of the differences between planktonic and biofilm bacteria has disclosed many important differences of relevance in this context between these two microbial states. Biofilm bacteria are not easily accessible to naive and immune host defence cells or soluble factors, such as complement or antibiotics (Costerton *et al*., 1999). Further, dormant pathogens embedded in the biofilm and adhering to the implant surface can be difficult to detach and grow in bacterial culture (Gristina and Costerton, 1985; Tunney *et al*., 1999). Therefore, different approaches have been developed to diminish false negative culture results, e.g. multiple sampling from the surface of the implant (direct swabs) and sonication of the implant to detach and disperse bacteria from implant surface to culture (Neut *et al*., 2003; Marculescu *et al*., 2005; Panousis *et al*., 2005; Trampuz and Widmer, 2006; Trampuz and Zimmerli, 2006; Zimmerli, 2006). None of these methods is perfect and the frequent use of antibiotics before sample collection further increases the risk for false-negative culture results (Darouiche, 2001; Berbari *et al*., 2007; Malekzadeh *et al*., 2010), but false-positive culture results are also possible, usually as a result of contamination during sample processing and culture.

Eukaryotic cells and bacteria produce various molecular components destined for extracellular deposition, which they excrete outside the cell. Eukaryotic cells synthesise components of extracellular matrix in their cytoplasm and secrete them via exocytosis.

Furthermore, adherent cells produce special adhesion organs known as focal adhesions (Konttinen *et al*., 2011). Also, bacteria excrete polymeric compounds, which form their extracellular polymeric substance (EPS), so called bacterial "slime" (Donlan, 2002). EPS is a polymeric conglomerate composed of extracellular DNA, proteins, and polysaccharides. We hypothesise that the molecular composition of the mammalian ECM and bacterial EPS differ to such an extent that modern and sensitive spectroscopic methods would enable their specific identification from cell-free footprints left on an implant surface after an effective removal of whole live and dead eukaryotic and bacterial cells. Because the cells, which produced them, are already gone, these acellular remnants left on their former growth substrate surface are hereafter referred to as "footprints". The aim of the work was to test two spectroscopic methods that might be useful for demonstration of previous bacterial colonisation, but in the absence of bacteria, and enable its differentiation from footprints left by human cells. Due to their role in implant-related infections (Cunningham *et al*., 2004; Trampuz and Zimmerli, 2006; Sohail *et al*., 2007), *Staphylococcus aureus* was selected as the model bacterium, and due to the role of mesenchymal stromal cells in healing of peri-implant tissue and implant integration (Chatterjea *et al*., 2010), MSC was selected as the model eukaryotic cell for these first "proof of the principle" studies. Titanium is a commonly used biomaterial and was therefore included in the study. Diamond like carbon (DLC) was selected in the study because of its anti-fouling properties (Page *et al*., 2009; Goto and Brunette, 2010). Based on our previous experiments, relatively weak footprints were expected because *S. aureus* and MSCs did not attach and spread on DLC surfaces as well as e.g. on cytocompatible Ti surface; for *S. aureus* 23 % coverage was reached on Ti *vs*. 0.4 % coverage on DLC (Levon *et al*., 2010). For MSCs 83% coverage was reached on Ti *vs*. 73 % coverage on DLC (Myllymaa *et al*., 2010). If it is possible to see differences in the bacterial, eukaryotic and joint (co-culture) footprints on DLC, it is very likely that the footprint analysis is rather sensitive and easily discloses differences in the footprints in other materials as well. Patterned materials were included to have a type of internal control (in the background material) and as a preliminary pilot to check if this study design could be used to demonstrate the 'race for the surface' phenomenon of bacterial and host cells (Gristina, 1987).

In recent years, ToF-SIMS has been employed for studying the surface of protein-based materials. Adsorbed protein films have been characterised (Lhoest *et al*., 2001; Wagner *et al*., 2001; Wagner *et al*., 2002a; Wagner *et al*., 2002b; Wagner *et al*., 2003a; Wagner *et al*., 2003b; Bernsmann *et al*., 2008; Tyler *et al*., 2011) and even conformational changes (Xia *et al*., 2002) and denaturation of proteins (Killian *et al*., 2011) can be detected with ToF-SIMS. Surface characterisations of extracellular matrix scaffolds (Canavan *et al*., 2007, Brown *et al*., 2010; Barnes *et al*., 2011) and insulin and albumin coated surfaces have been published (Henry and Bertrand, 2009). In the field of microbiology, ToF-SIMS has been applied to imaging colonies of microbes (Tyler *et al*., 2006, Esquenazi *et al*., 2009), to characterise intact, individual bacterial spores in 3D (Ghosal *et al*., 2008) and to detect antibiotics within intact bacterial colony biofilms (Gasper *et al*., 2008). Some previous experiments have applied TOF-SIMS to cellular material and have successfully discriminated between different yeast strains (Jungnickel *et al*., 2005) and different breast cancer cell types (Kulp *et al*., 2006). Here, we extend these earlier findings further, attempting to distinguish between two different cell types based on their footprints, following detachment of the cells from their matrix, rather than trying to distinguish the cells themselves. Although it has been shown before that after cell sheet detachment, traces of amino acids are found on the culture substrate (Canavan *et al*., 2005a; Canavan *et al*., 2006), identification of different cells based only on these cellular footprints on biomaterial has never been attempted before by ToF-SIMS experiments.

Materials and Methods

Sample fabrication

DLC and titanium were deposited on silicon surfaces, both as planar coating and patterned coating. The samples contained regularly spaced 75 µm x 75 µm squares covered with titanium or DLC squares with the distance of 100 µm. Patterning was produced using photolithography and lift-off techniques.

Thin films of titanium were magnetron sputtered (Stiletto Serie ST20, AJA International Inc., North Scituate, MA, USA) in argon plasma with high purity (99.9 % or better) target materials (Goodfellow Metals, Huntingdon, UK). An acceleration voltage of 400-500 V, a chamber pressure of 3-4x10^{-4} mbar and a deposition time of 5 min were used to deposit approximately 200 nm thick films.

DLC coatings were deposited using ultra-short pulsed laser deposition (USPLD) technique. Just before deposition, the sample surfaces were gently cleaned using Ar^+ ion sputtering (SAM-7KV, Minsk, Belarus). For deposition, we used a new type of mode-locked fibre laser (Corelase, Tampere, Finland) and Coldab™ deposition technology developed by Picodeon (Helsinki, Finland) to achieve optimal laser parameters in USPLD (Myllymaa *et al*., 2009). The maximum average power was 20 W at 4 MHz which results in a 5 µJ pulse energy. The pulse length was 20 ps. High purity graphite was used as the target for DLC deposition. The deposition parameters were adjusted to obtain stable plasma and to deposit about a 150 nm thick layer.

After deposition, the patterns on wafers were revealed by immersion in a mr-Rem 660 resist remover (Microresist Technology, Berlin, Germany) in an ultrasonic bath for a few minutes. Wafers were finally cut to 10 mm x 10 mm samples before sonication for a few minutes in 7x detergent (OneMed, Vantaa, Finland), ethanol and deionised water to remove organic residues and silicon dust from dicing.

Sample sterilisation

Samples were immersed in Petri dishes for 30 min in 70 % ethanol, which was removed by pouring and evaporation before packaging in sterile bags and sterilisation using

26 ±3 kGy gamma irradiation. The source was calibrated according to ASTM 1026-95 Standard Method for Absorbed Gamma Radiation Dose in the Fricke Dosimeter.

Measurement of zeta-potential

Zeta-potentials were measured using an electrokinetic analyser (SurPASS, Anton Paar, Graz, Austria) in pH 7.1 ±0.1 in 1 mM KCl. The samples were measured in duplicates (i.e., two pairs) using an adjustable gap cell on which the samples were mounted and the measurements were repeated three times for each pair. The zeta-potential was evaluated from streaming current measurements according to the Helmholtz-Smoluchowski equation:

$$\zeta = \frac{dl}{dP} \times \frac{\eta}{\varepsilon \times \varepsilon_o} \times \frac{L}{A}$$

Where ζ is the zeta-potential; *dl/dP* is the slope of streaming current *vs*. different pressure; η is the electrolyte viscosity; ε is the permittivity; ε_o is the dielectric coefficient of electrolyte; and *L* is the length of streaming channel and *A* is its cross-section. Error estimation was based on the standard error of the mean.

Cell cultures

Human bone marrow-derived passage-5 MSC (PoieticsTM, Lonza, Basel, Switzerland) were cultured on 10 cm Petri dishes (Corning, Corning, NY, USA) using Lonza Mesenchymal Stem Growth Medium (MSCGM) containing Mesenchymal Cell Growth Supplement, L-Glutamine and GA-1000 (Gentamicin/Amphotericin-B). The cells were cultured at 37 °C in humid 5 % CO_2-in-air. The cell monolayer was washed with phosphate buffered 140 mM saline (PBS, pH 7.4) and the cells were detached using 2.5 mg/mL trypsin in PBS-EDTA (0.05 mL/cm^2) at room temperature for 5 min. An equal volume of temperature equilibrated MSCGM was added. The suspension was transferred to a Falcon tube and trypsin was removed by centrifuging the cells at 600 g for 5 min. Cells were resuspended in culture medium and seeded onto the pre wetted biomaterial surfaces at 6000 cells per cm^2 density. The cells were cultured for 6 days (near confluence). TC-treated polystyrene 12-well microplates (Corning) were used in all experiments. A similar protocol was followed when the control samples without cells were prepared.

Bacterial cultures

A biofilm producing strain of *S. aureus* S-15981, kindly provided by Dr. Lasa (Valle *et al*., 2003), was cultured on blood agar for 24 h at 37 °C under aerobic conditions. Twenty colony forming units (CFU) were suspended into 10 mL tryptic soy broth (TSB) and cultured for 24 h at 37 °C in a 15 mL tube (with static agitation). This suspension was re-suspended and 1 mL was inoculated into 9 mL of TSB and incubated for 18 h at 37 °C. Thereafter, the concentration was adjusted to 6 × 10^8 CFU/mL using a McFarland standard and verified by serial dilution plating. Biomaterial samples placed in the wells of pre-sterilised, polystyrene, flat-bottomed, 12-well microplates (Corning) were pre-wetted with TSB and covered with 1 mL of the microbial solution and incubated for 24 h at 37 °C. Then, medium was aspirated and non-adherent cells removed by thoroughly washing the biofilms three times in sterile PBS, covered with 1 mL of TSB and incubated for another 24 h at 37 °C. During the incubation samples were agitated gently using a GrantBioPMS 100 microplate shaker. Non-infected wells (TSB alone) were also included to serve as negative controls.

Co-cultures

Two types of co-cultures were prepared in MSCGM without antibiotics. In the first set-up, MSCs were suspended in MSCGM and seeded on the biomaterial surfaces placed in 12-well microplates at 6000 cells per cm^2 density and cultured for 48 h at 37 °C in humid 5 % CO_2-in-air. After 48 h, the surfaces were covered with S-15981 *Staphylococcus* solution at concentration of 6 × 10^8 CFU/mL in MSCGM and incubated for 48 hours at 37 °C. After 24 h the suspension was refreshed with 500 µL of MSCGM.

In the second set-up, both MSCs and S-15981 were suspended in MSCGM using similar seeding densities (6000 MSCs per cm^2) and concentration (6 × 10^8 CFU/mL) as above. Biomaterial surfaces were placed in 12-well microplates, followed by addition of 1 mL of the mixed *Staphylococcus* and MSC solution. These co-cultures were incubated for 96 h at 37 °C. Refreshing was done every 24 h, by replacing 500 µL of the culture solution with fresh MSCGM.

Viability in co-cutures

Bacterial viability in MSCGM was confirmed with staining using Live/Dead BacLight™ kit (Molecular Probes/Life Technologies, Gaithersburg, MD, USA), which was applied according to manufacturer's instructions and analysed using fluorescence microscopy.

To assess the amount of biomass in a biofilm, *S. aureus* was cultured in MSCGM and in TSB on 24-well plates for 96 h, washed with PBS, dried for 30 min at room temperature and stained in 200 µL of 0.3 % crystal violet (Reagena Ltd., Toivala, Finland) for 5 min. Samples were washed gently in running water and destained in 200 µL of absolute ethanol, which was transferred to a clean 96-well plate. Absorbance at 544 was measured with Plate CHAMELEON V (Chameleon Systems, Ruislip, UK) plate reader.

To test the viability of MSCs in co-cultures, samples were prepared on coverslips using the same experimental settings as described above. After the co-culture incubation, Live & Dead staining was performed using the Live/Dead Viability/Cytotoxicity Kit for mammalian cells (Molecular Probes). Samples were washed with PBS, stained with MSC-optimised staining solution (8 µM calcein acetomethoxy and 2 µM Ethidium Homodimer-1) for 40 min, washed with PBS and mounted in Vectashield (Vector Laboratories, Peterborough, UK).

Live & Dead staining was observed using Leica DM6000 B/M Research Microscope equipped with a DFC365FX camera (Leica Microsystems, Wetzlar, Germany).

Surface cleaning

The seeding density and culture times for both MSCs and *S. aureus* were selected so that the culture was near confluence before surface cleaning. Surfaces were washed three times in PBS. Cells and bacteria were trypsinised (1:10 trypsin in PBS-EDTA) 5 min at 37 °C, after which the trypsin was neutralised with equal amount of trypsin neutralisation solution (PromoCell, Heidelberg, Germany). Samples were washed three times with dH_2O and sterilised in abs. ethanol. The samples were soaked in dH_2O for at least 24 h to reduce free ions remaining from the buffer after which the liquid on the sample was removed using the N_2 gas.

Scanning electron microscopy (SEM)

To ensure that the surfaces were well cleaned from cells and bacteria the samples were imaged with a Hitachi (Tokyo, Japan) SEM FE 4800 field emission scanning electron microscope (FE-SEM) without any additional surface treatments at an accelerating voltage of 10 kV.

X-ray photoelectron spectroscopy (XPS)

XPS measurements were conducted on X-ray photoelectron spectrometer (PHI 5600) using monochromated Al Kα radiation (1486.6 eV, 300 W) for excitation. The spectra of the elements were determined at a pass energy of 23.5 eV and a total energy resolution of < 0.4 eV, and values were recorded every 0.1 eV and at a takeoff angle of 45° with respect to the surface normal. XPS was performed only for planar titanium and DLC surfaces. To interpret XPS data, linear least square fit of Gaussian functions were fitted to the high-resolution oxygen, nitrogen and carbon spectra (Matlab, Mathworks, Natick, MA, USA).

Time of flight secondary ion mass spectrometry (ToF-SIMS)

Positive and negative static ToF-SIMS measurements were performed using a ToF-SIMS V spectrometer (ION TOF, Münster, Germany). The samples were irradiated with a pulsed 25 keV Bi^+ liquid-metal ion beam. The beam was electrodynamically bunched down to 25 ns to increase the mass resolution and rastered over a 500 x 500 μm^2 area. For patterned samples measurements were carried out separately from pattern and background, from an area of approx. 70 x 70 μm^2. The primary ion dose density (PIDD) was kept at approximately 5 x 10^{11} ions x cm^{-2}, ensuring static conditions. Signals were identified using the accurate mass as well as their isotopic pattern. In this article, only the positive ToF-SIMS spectra are presented because they contain a greater amount of information regarding our area of interest.

Based on the preliminary analysis of the ToF-SIMS spectra, 11 components that showed difference between MSC and *S. aureus* samples were selected for ToF-SIMS imaging. The components were m/z 39 K, 70 C_4H_8N, 73 $C_4H_{10}N$, 74 C_3H_8NO, 86 $C_5H_{12}N$, 91 C_7H_7, 101 $C_4H_9N_2O$, 110 $C_5H_8N_3$, 120 $C_8H_{10}N$, 130 C_9H_8N and 136 $C_8H_{10}N$.

Principal component analysis (PCA)

First, all spectra were mean-centred prior to principal component analysis. A limited peak set was constructed

Table 1: List of characteristic secondary ions fragments cleaved off from amino acids for mass spectrometric analysis.

Mass		Formula	Amino acids
30	*	CH_4N	Gly, Lys
42	*	C_2H_4N	Ala, Gly, His, Leu, Ser
43	*	CH_3N_2	Arg
		C_3H_7	Leu, Ile
44	*	CH_4N_2	Arg
		C_2H_6N	Ala, Lys, Asp, Leu
45		CHS	Cys
47		CH_3S	Cys
54		C_3H_4N	His
55		C_3H_3O	Tyr
58		C_2H_4NO	Gly
		C_3H_8N	Glu
59		CN_3H_5	Arg
60		C_2H_6NO	Ser
61		C_2H_5S	Met
68		C_4H_6N	Pro
69		C_4H_5O	Thr
70	*	C_3H_4NO	Asn
		C_4H_8N	Arg
71		$C_3H_3O_2$	Ser
72		C_3H_6NO	Gly
		$C_4H_{10}N$	Val
73		$C_2H_7N_3$	Arg
74		C_3H_8NO	Thr
81		$C_4H_5N_2$	His
82		$C_4H_6N_2$	His
83		C_5H_7O	Val
84		C_4H_6NO	Gln, Glu
		$C_5H_{10}N$	Lys
85		$C_3H_5N_2O$	Gly
86		$C_5H_{12}N$	Ile, Leu
87		$C_3H_7N_2O$	Asn
88		$C_3H_6NO_2$	Asn
91		C_7H_7	Phe, Tyr
95		$C_5H_7N_2$	His
98		$C_4H_4NO_2$	Asn
100		$C_4H_{10}N_3$	Arg
101	*	$C_4H_{11}N_3$	Arg
		$C_4H_9N_2O$	Gln
		$C_5H_{12}N_2$	Lys
102		$C_4H_8NO_2$	Glu
104		$C_4H_{10}NS$	Met
107		C_7H_7O	Tyr
110		$C_5H_8N_3$	His
113		$C_4H_5N_2O_2$	Gly
115		$C_4H_7N_2O_2$	Gly
120		$C_8H_{10}N$	Phe
121		$C_6H_5N_2O$	His
127		$C_5H_{11}N_4$	Arg
129		$C_5H_{13}N_4$	Gln
130		C_9H_8N	Trp
131		C_9H_7O	Phe
132		C_9H_8O	Phe
136		$C_8H_{10}NO$	Tyr
159		$C_{10}H_{11}N_2$	Trp
170		$C_{11}H_8NO$	Trp

* not included in the analysis.

to compare the positive ToF-SIMS spectra from all sample types. This limited peak set was constructed using unique amino acid fragmentation patterns of ToF-SIMS data previously identified for characterising proteins. Table 1 shows the selected peaks together with the amino acid they are characteristic for and the proportion of that amino acid (Samuel *et al*., 2001; Wagner and Castner, 2001; Canavan *et al*., 2006; Henry and Bertrand, 2009). Peaks that can originate from several different amino acids (marked with a star in Table 1) were not included in the analysis. The peak areas for each spectrum were then normalised to the intensity of the sum of the selected peaks to account for fluctuations in secondary ion yield between different spectra. Then, the data of MSCGM was subtracted from MSC-data and co-culture data and the data of tryptic soy broth was subtracted from *S. aureus* data. PCA was used to analyse the ToF-SIMS spectra (Matlab, MathWorks) of MSC and bacteria footprint. Coefficients obtained from PCA were applied then also to the co-culture data. To further elucidate differences between the groups, the data were analysed with Mann-Whitney U-test (SPSS, Chicago, IL, USA).

Patterned DLC-samples were not included in the PCA analysis as our previous study showed that after 90 min long adhesion experiment only 0.38 % of the patterns and 0.40 % of the background was covered with *S. aureus* and thus hardly any footprint can be expected (Levon *et al*., 2010).

Results

Zeta-potential

DLC has the lowest zeta-potential (-54.5 ±0.6 mV) and Ti the highest (-40.9 ±0.9 mV) and Si an intermediate (-46.7 ±0.5 mV) zeta-potential.

SEM

SEM images showed that surfaces were well cleaned from cells and bacteria (Fig. 1).

Viability

As a control, it was important to show that S-15981 *Staphylococci* grow effectively and produce EPS, both in this MSCGM medium and with this culture time. This was confirmed by Live & Dead staining (not shown), which showed that *Staphylococci* grew effectively. The volume of EPS produced was measured by using absorbance of crystal violet to the biofilm formed. These experiments indicated that the amount of biomass of the biofilm produced in MSCGM during this culture time was similar to that produced in the TSB culture medium (absorbance at 544 was 1.4 ±0.3 in TSB, 1.3 ±0.3 in MSCGM and 0.3 ±0.02 for negative controls).

In co-culture type 1, where *S. aureus* and MSCs were added simultaneously, almost all MSCs were detached from the surface after 96 h of co-culture. In co-culture type 2 some MSCs were still viable (not shown).

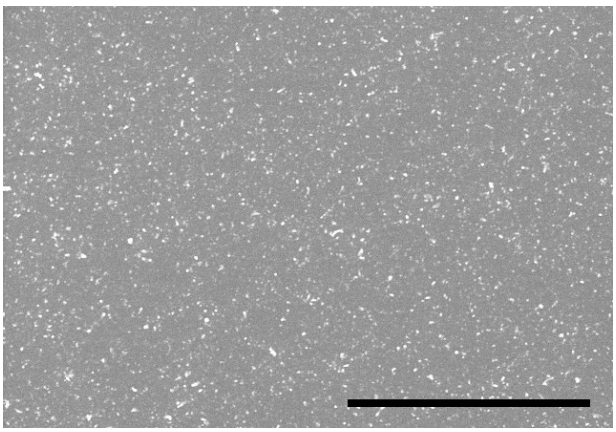

Fig. 1. Scanning electron microscopy image of the surface showing that after the procedure used for the detachment of the bacterial and mammalian cells from the implant surface, no bacterial and eukaryotic cells remain attached to surface. Scale bar is 10 µm.

XPS

The quantitative results from XPS analysis are shown in Table 2. In general, the XPS spectra exhibited peaks from oxygen, carbon and nitrogen. In addition, the Ti-samples naturally had the spectra of Ti2p.

The hydrocarbon (C-C and C-H; Fig. 2) peak is located at 284.2 eV, the ether and alcohol contributions (C–O–C and C–O–H) at 286.0 eV, acetal carbon (O–C–O) at 288.3 eV and the ester group at 288.8 eV (C–O–C=O and O–C=O).

The spectra of N1s exhibited a peak with a binding energy of about 400 eV, indicating that nitrogen was present in the organic matrix, probably as amino groups, most likely originating from amino acids.

The high oxygen peak originates from oxidation of the surface and the shoulder appearing at a binding energy 1.4-1.6 eV higher than the main O 1s peak originates from ether (C-O-C), alcohol (C-O-H) and ketone oxygen (C=O). The small shoulder at 533.7 eV indicates carbonyl- and ether-type oxygen in ester (O=C-O-C).

Only a few differences were observed between Ti-samples. MSC samples have relatively higher amount

Table 2: The relative atomic concentrations of carbon, nitrogen, oxygen, and titanium are presented from x-ray photoelectron spectroscopy measurement.
Mesenchymal stem cell (MSC), growth media (GM), tryptic soy broth (TSB).

Sample	C1s	N1s	O1s	Ti2p
Ti MSC	48.03	4.35	35.45	12.17
Ti MSC-GM	44.64	7.42	36.35	11.59
Ti *S. aureus*	51.24	6.92	32.93	8.90
Ti TSB	43.29	6.31	37.41	13.00
DLC MSC	74.63	8.81	16.55	
DLC MSC-GM	75.92	8.39	15.70	
DLC *S. aureus*	74.57	9.19	16.24	
DLC TSB	73.78	7.19	19.03	

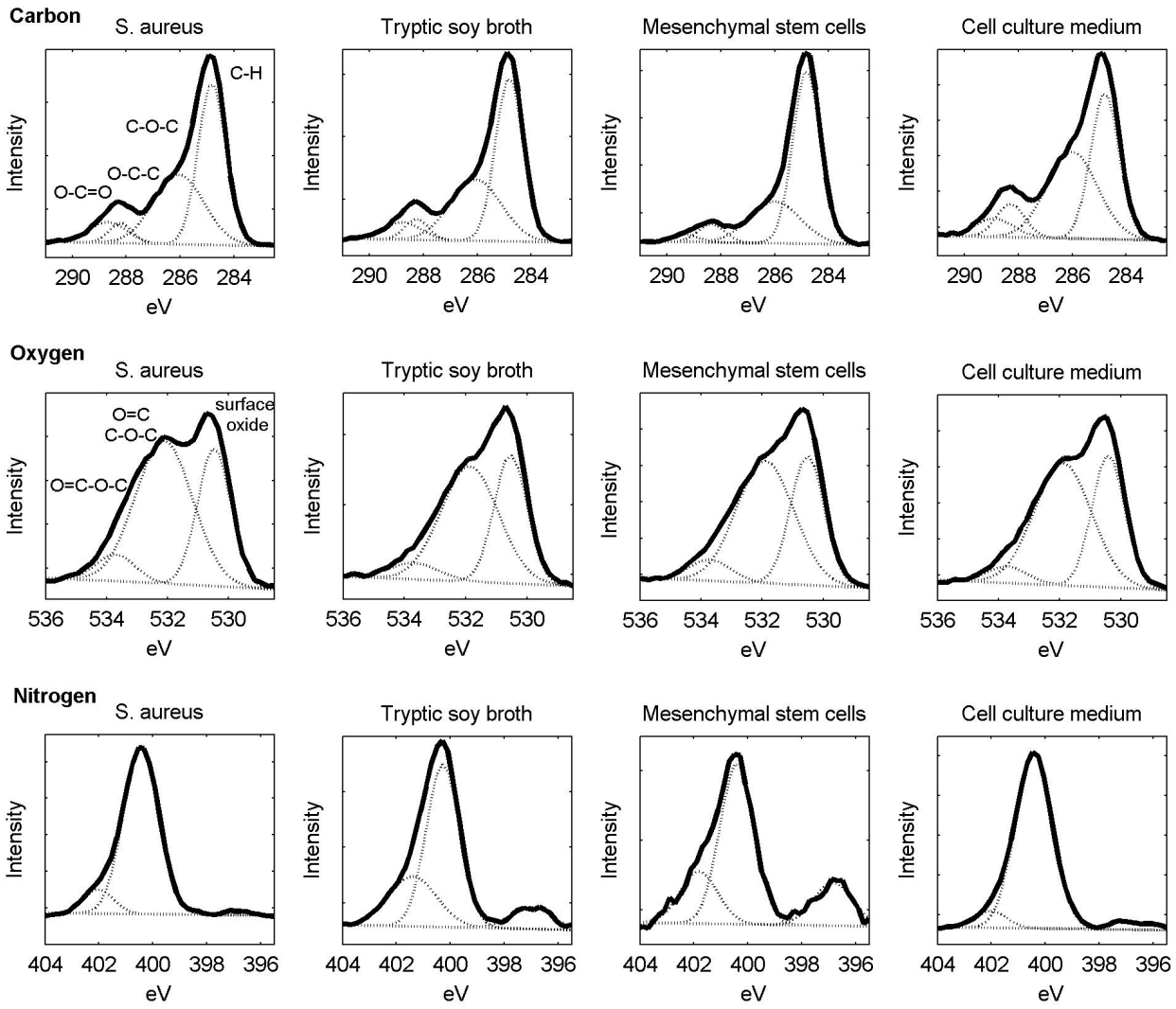

Fig. 2. X-ray photoelectron spectroscopy of carbon, oxygen and nitrogen on Ti surfaces subjected to *Staphylococcus aureus* and mesenchymal stem cell cultures and their media.

of hydrocarbon (68.5 % of C1 peak while others have < 56.5 %), lower amount of carbon in ester groups (1.4 % of C1 compared to > 4.0 % of other samples) and higher amount of energy at 397 eV compared other samples (16.2 % of N1s compared to > 8.6 % of other samples). On *S. aureus* samples the second O1 peak is a little shifted being 1.6 eV higher than the main O 1s peak (532.1 eV compared to 531.9 eV of the other samples). This indicates that *S. aureus* sample surface contains more ether and alcohol oxygens than ketone oxygens when compared to other samples. However, these differences are not sufficient for separating *S. aureus* samples from MSC samples.

ToF-SIMS

The PCA of the ToF-SIMS data allowed clear overall separation ($p < 0.03$) of *S. aureus* samples and co-culture samples from MSC-samples (Fig. 3A; representative samples). The differences were predominantly observed in principal component (PC) 1, which accounted for 66 % of the statistical separation of the total variance between all samples. Logically, the PCA values of co-cultures locate between the values of pure MSC-samples and pure *S. aureus* samples. Furthermore, the co-culture type 1 (started with MSC culture) was further away from *S. aureus* than the co-culture type 2 (to which MSC and *Staphylococci* were added simultaneously), with one exception. Titanium patterns showed a much stronger *S. aureus* footprint in co-cultures than in pure *S. aureus* culture.

It was observed that the peaks at m/z 72 (C_3H_6NO glycine, $C_4H_{10}N$ valine), 84 ($C_5H_{10}N$ lysine, C_4H_6NO glutamine / glutamic acid) and 86 ($C_5H_{12}N$, leucine / isoleucine) accounted for most of the loading on the *S. aureus* site of the PC 1 axis while peaks at m/z 45, 47 (CHS, CH_3S cysteine) and 81 ($C_4H_5N_2$, histidine) accounted for most of the loading on the side of the PC 1 axis attributed to the MSC-samples (Fig. 3B). The MSCs expressed more histidine than *S. aureus* and culture on the patterned Ti surfaces showed a clear structure of the main histidine component (110; Fig. 4A).

In PC 2, which accounted for 19 % of the statistical separation of the total variance between all samples, the only component accounting over 20 % weight was m/z 45

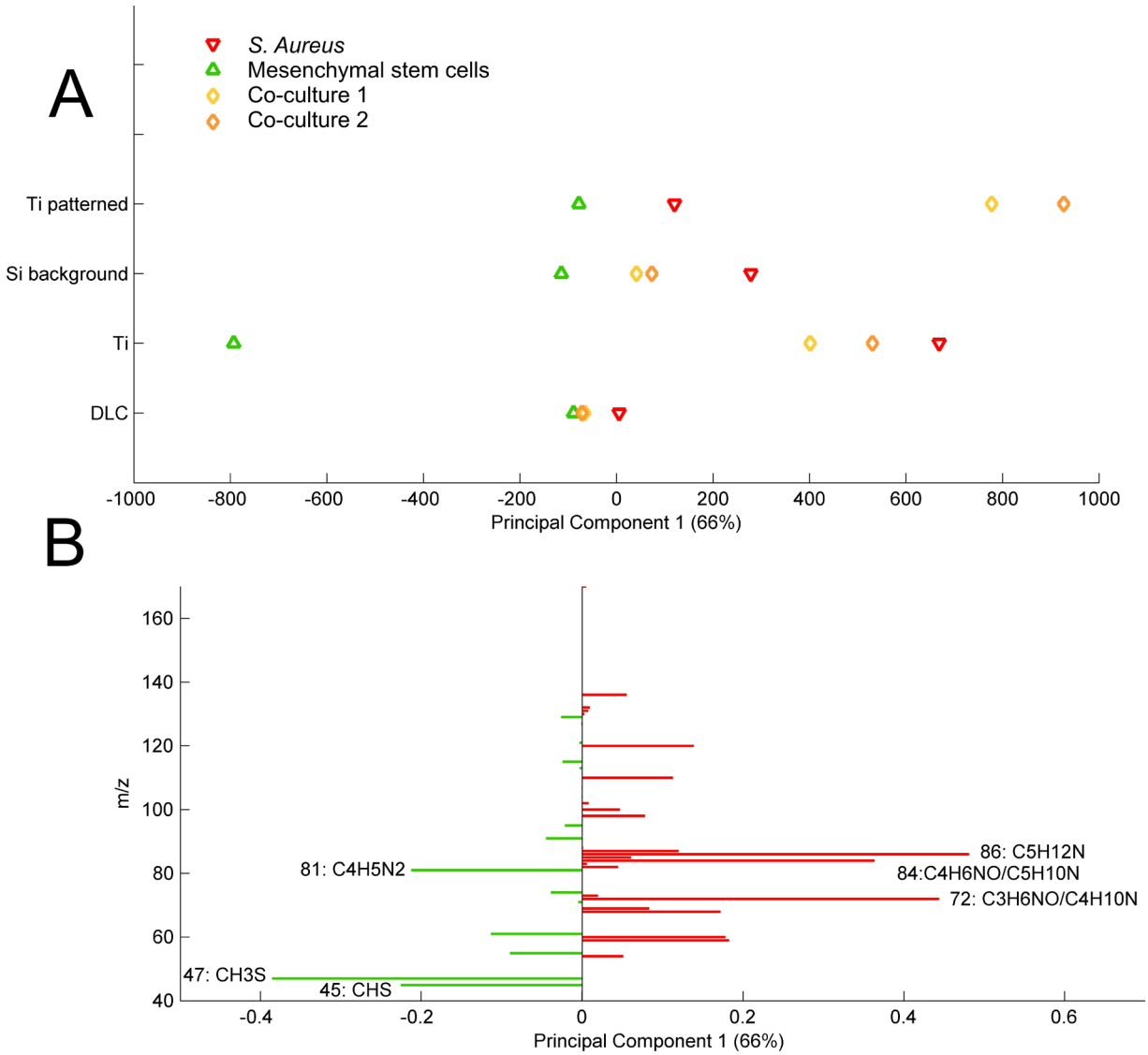

Fig. 3. Results of principal component analysis (PCA). (**A**) Scores of PCA. The *Staphylococcus aureus* and co-culture footprint are clearly separated from the mesenchymal stem cell footprint. In co-culture 1, MSCs were cultured on the surfaces 48 h prior to seeding of *S. aureus*. In co-culture 2, MSCs and *S. aureus* were seeded at the same time. Measurements were performed on patterned titanium on silicon background and on pure titanium and diamond like carbon (DLC) surfaces. (**B**) Loads of PCA. Components counting over 20 % loads are named. It was observed that the peaks at m/z 72 (C_3H_6NO, $C_4H_{10}N$), 84 ($C_5H_{10}N$, C_4H_6NO) and 86 ($C_5H_{12}N$) accounted for most of the loading on the *S. aureus* site of the PC1 axis while peaks at m/z 45 (CHS), 47 (CH_3S) and 81 ($C_4H_5N_2$, histidine) accounted for most of the loading on the side of the PC 1 axis attributed to the MSC-samples.

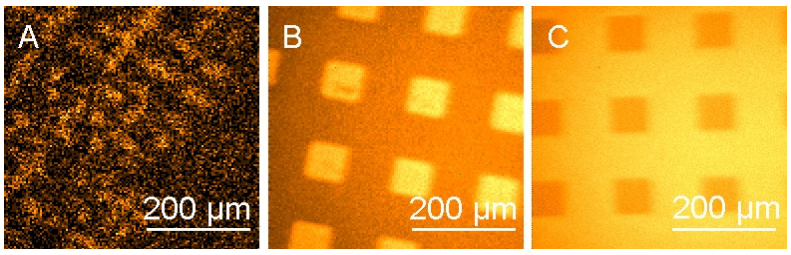

Fig. 4. Adsorption visualised with a time of flight secondary ion mass spectrometer. (**A**) After mesenchymal stem cell culture component 110 (histidine) shows a clear structure on titanium. (**B**) Titanium patterns adsorbs more molecules than silicon background (total ion count) but (**C**) DLC patterns adsorb less molecules than silicon background (total ion count).

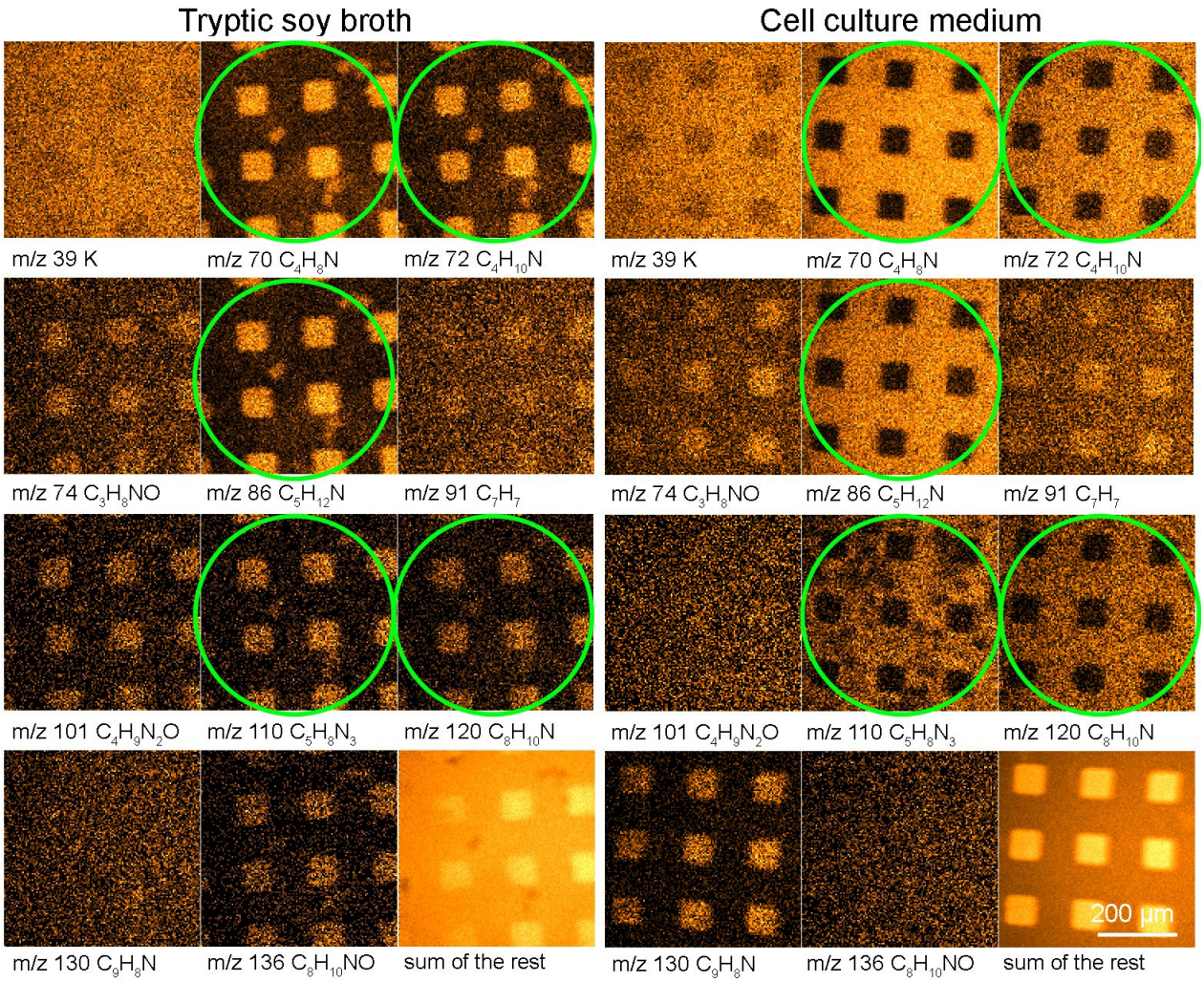

Fig. 5. Adsorption of tryptic soy broth and mesenchymal stem cell culture medium on patterned titanium sample visualised with a time of flight secondary ion mass spectrometer. Differences between the two media are circled.

(CHS, 93 %) and it was predominantly associated with differences between MSC sample and *S. aureus* sample on silicon background, accounting for most of the m/z 45 (CHS) loading to the MSC site of the PC 2 axis (not shown).

ToF-SIMS results demonstrated interesting 'race for the surface' (Gristina, 1987) phenomenon on patterned Ti-samples. The cell culture media mass components 70 (C_3H_4NO, C_4H_8N), 72 (C_3H_6NO, $C_4H_{10}N$), 86 ($C_5H_{12}N$), 110 ($C_5H_8N_3$) and 120 ($C_6H_5N_2O$) preferred the Si-background over the Ti-patterns. The same mass components of bacterial culture medium TSB showed the opposite preference, preferring the Ti-patterns over the Si-background (Fig. 5). On the patterned DLC-samples the selected components of TSB showed similar adsorption as on the patterned Ti-samples except for the mass component 91, which showed the opposite preference; it clearly preferred the Si-background over the DLC-patterns (Fig. 6). However, the cell culture medium showed different adsorption preference on the patterned DLC-samples from that on the patterned Ti-samples. From the components that were imaged this opposite preference can be seen for components 70, 72, 86, 91 (C_7H_7), 110, 120 and 130 (Fig. 6). Intriguingly, the total ion preference on patterned Ti-samples was on the Ti-patterns but on the patterned DLC-samples the ions preferred the Si-background (Fig. 4B, C).

The surfaces exposed to cell and bacteria showed similar but more blurred preferences as their culture media. The exception was that on patterned Ti-samples the preference of potassium (39) changed and histidine (the histidine-derived mass component m/z 110 $C_5H_8N_3$) showed a clear structure (Fig. 4A).

Discussion

We hypothesised that XPS spectra, obtained by focused x-ray irradiation of the footprints on the implant surface and analysis of the number and kinetic energy of the detached (emitted) photoelectrons, could be used in the recognition of cellular footprints. XPS has been earlier used to detect differences in the amounts of calcium and phosphorous as a sign of mineralisation on the culture substrate before and after osteoblast culture (Mustafa *et al.*, 2002). XPS is also suitable for recognition of different

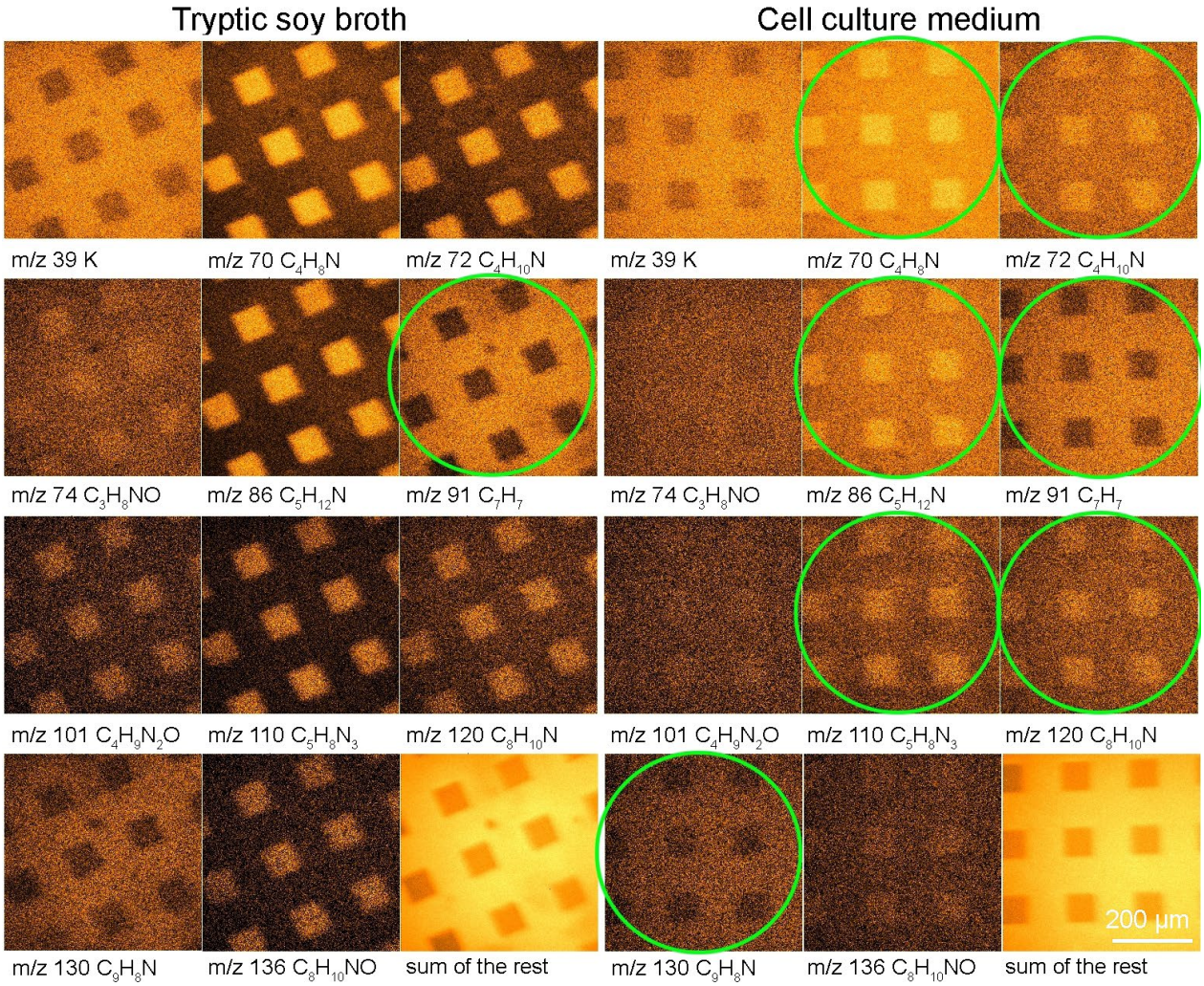

Fig. 6. Adsorption of tryptic soy broth and mesenchymal stem cell culture medium on patterned diamond like carbon sample visualised with a time of flight secondary ion mass spectrometer. The differences of adsorption, compared to patterned titanium sample, are circled.

monosaccharides, disaccharides, and polysaccharide (Stevens and Schroeder, 2009). However, in our study, with a much more complex ECM and EPS as the study objects, only minor differences were observed between MSC- and *S. aureus*-culture samples so that a reliable separation of them was impossible. This could be expected due to the relatively non-descript nature of XPS compared to SIMS analysis of protein-adhered surfaces, as has been well-described in the literature (Wagner and Castner, 2001; Canavan *et al*., 2005b).

ToF-SIMS is obtained by focusing a pulsed primary ion beam onto the footprints on the implant surface and analysis of the number and mass of the detached secondary ions, as well as for a reconstruction of a topographical map on their localisation on the surface of the target of the ion beam, that is, of the implant and footprint surface. In contrast to XPS, this method seems to have potential for separation of mammalian and bacterial footprints. Some previous experiments have applied TOF-SIMS for cellular material and have successfully discriminated, for example, between different yeast strains (Jungnickel *et al*., 2005), different breast cancer cell types (Kulp *et al*., 2006) and living and dead bacterial cells (Tyler *et al*., 2006). These studies, however, are significantly different from ours as they studied the actual cellular materials whereas we used TOF-SIMS to discriminate the infected surfaces from the non-infected surfaces after careful cleaning and removal of the cellular material (cells) from these surfaces. Not quite surprisingly, the footprints produced were affected by the substrate material used for culture. This might have contributed to the difference observed between MSC- and *S. aureus*-produced ECM and ESP remnants, respectively.

It has been earlier shown that both MSCs and *S. aureus* spread better on Ti surfaces than on DLC surfaces. In 5-day MSC cultures on patterned surfaces, 82.7 % of Ti- and 72.7 % of DLC-patterns were covered by MSCs (Myllymaa *et al*., 2010). In 16 h *S. aureus* cultures, 100 % of the planar Ti but only 81.05 % of the planar DLC surface was covered by bacteria ($p < 0.001$) (Levón *et al*,. unpublished results). This better adherence and growth of both types of cells on

the "sticky" titanium may in part explain why the MSC and *S. aureus* footprints were more easily differentiated on Ti than on DLC samples.

Another potential explanation for the differences in the TOF-SIMS footprints between Ti and DLC surfaces is that the Ti surface binds more proteins and amino acids than the Si-background and that the DLC surface binds less of these components than the Si-background (Fig. 4). This was demonstrated by the ToF-SIMS images of patterned Ti and DLC samples, where the total ion count was significantly higher on the Ti-patterns than on the Si-background, whereas on the DLC-patterns the total ion count was lower than on the Si-background. The differential binding of proteins and amino acid on these two surfaces may, for some compounds, result in part from the differences of the zeta-potential values of these samples. It has been earlier demonstrated that the lower the absolute value of the zeta-potential (measured in 0.001 M KCl) of the surface is, the lower is the adsorption of serum proteins on it (Cai *et al*., 2006). However, these studies were conducted on surfaces, which had zeta-potentials within a relatively narrow range of only -12 to 0 mV. Indeed, typically the streaming current measurements are performed in KCl because use of culture media would contaminate the electrokinetic analyser used to measure zeta potential. Zeta-potential of the samples would certainly be different e.g. in the cell culture media. Therefore, correlation between protein adsorption and zeta-potential value measured in KCl is disputed and, according to the above mentioned work, zeta potentials measured in 1 mM KCl only reflect the protein binding capacity of the test surfaces. Evidence has been recently presented that a parabolic relationship exists between the protein adsorption and zeta-potential when a much wider zeta-potential range is taken into consideration (Shin *et al*., 2008; Kaivosoja *et al*., 2011).

In co-culture type 1, where *S. aureus* and MSCs were added simultaneously, there were no longer MSCs present after 96 h incubation. In co-culture type 2, where MSCs were first allowed to adhered and grow for 48 h before the addition of *S. aureus*, there were some viable and adherent cells left on the culture substrate. Although the conditions were not optimal for co-habiting the sample surface, they simulate the situation in implant-related infections well. Presence of adhering bacteria, which produce biofilm and exotoxins, diminishes the substrate area covered by eukaryotic cells (Saldarriaga Fernández *et al*., 2011a; Saldarriaga Fernández *et al*., 2011b). Even though most of the MSCs had detached from the surface at 48 h, they had left their footprint on the surface on which they had 'raced for the surface' with bacteria, and this was what we aimed for with these co-culture experiments. Non-optimised conditions may lead to stressed phenotypes causing deposition of stressed matrix proteins on surfaces, so it is possible that the differential in adhesion observed is a result caused by the stressed conditions. This does not undermine the hypothesis, but it may modify the outcome observed. In patients the situation is somewhat different, because new cells can be continuously recruited to the implant surface. Bacterial growth on implant surface starts with low colony forming unit numbers and, because many implant-related infections are haematogenous, the host cells have had time to establish themselves on the implant surface. More importantly, it was possible to find evidence for a previous growth of bacteria in form of clearly detectable bacterial footprints on these samples, which no longer contained any bacterial cells, only remnants of their EPS. The topographical ToF-SIMS maps show that the *S. aureus* footprints express more valine, lysine, glutamine, glutamic acid, leucine, isoleucine, tyrosine and tryptophan as well as less cysteine and histidine than the MSC footprints. However, care must be taken when assigning ToF-SIMS mass peaks exclusively to particular amino acids. This is particularly true for the small molecular mass components, such as CH_4N (m/z 30) mass peaks, which can produce a very high signal from every amino acid. C_9H_8N (m/z 130) suggests the presence of tryptophan in the footprint, but forms also the 3rd most abundant peak produced by glutamine (Kulp *et al*., 2006). Furthermore, the influence of the closest neighbouring molecules in the protein structures on the ion beam induced fragmentation of the amino acids is difficult to predict. In spite of some such difficulties in the exclusive identification of the molecular mass peaks produced, the main point is that the footprints of MSC and *S. aureus* samples can be separated from each other using these ToF-SIMS spectra. This separation was clear on sticky titanium surfaces, but was possible even on DLC surfaces that are considered to be antifouling.

The reason that ToF-SIMS shows much higher signals attributed to *S. aureus* on most surfaces is logically associated with the *S. aureus* dominance likely to be found in co-cultures and rapid killing of mammalian cells in these cultures, as well as consistent surface dominance of bacteria in such cultures. However, the question is not about the signal intensity but about the differential signals (marks, footprint) left by bacterial and eukaryotic cells, which could provide evidence of previous bacterial colonisation and biofilm formation of bacteria-free implant surfaces.

ToF-SIMS images demonstrated an interesting 'race for the surface' (Gristina, 1987; Santavirta *et al*., 1992) type of phenomenon on patterned Ti-samples for proteins. Binding of certain ToF-SIMS components, e.g. m/z 70, 110, of the MSCGM and TSB were different on similarly patterned Ti-samples. Pattern contrast observed with ToF-SIMS is a function of the types and thicknesses of proteins adsorbed from the different culture milieu (or locally produced by the cells attached to the surface), which is influenced by the substrate. The total (secondary) ion preference of both media was on the Ti-patterns on the patterned Ti-samples. Nonetheless, individual components show different preferences. Figure 5 demonstrated that components m/z 70, 72, 86, 110 and 120 of TSB preferred Ti-patterns over Si-background, but the same components of MSCGM preferred Si-background. In conclusion, the MSC growth medium contains some components that occupy the more favourable Ti on patterned surfaces, so that no space remains for the competing components. These other components lost the 'race for the surface' (e.g., m/z 70, 72, 86, 110 and 120) and were not found on the Ti on the patterned surfaces. This theory is supported by the finding that on the patterned DLC-samples (where the total ion preference was on Si-background) these very

same components were again forced to attach on the less favourable surface, namely on the DLC on the patterned surfaces.

The 'race for the surface' phenomenon can partly explain why the *S. aureus* footprint produced in co-cultures on titanium-patterns was in fact stronger than the footprint of pure *S. aureus* on titanium-patterns. Previous experiments have shown that *S. aureus* favours binding to Ti-patterns over the Si-background (22.7 % coverage on the Ti-patterns *vs*. only 0.7 % coverage on the Si-background (Levon *et al*., 2010)) whereas the difference for the MSCs is much lower (31 % coverage on Ti-patterns *vs*. 24 % coverage on Si-background (Myllymaa *et al*., 2010)).

The change in the preference for topological binding sites of potassium (39), on patterned Ti-samples, on a Si-background before MSC-culture and on Ti-patterns after the MSC-culture indicates that MSCs prefer the Ti-patterns over the Si-background and leave a potassium-enriched footprint. Potassium is possibly derived from intracellular sources, where it is present at 135-150 mmol/L (Girgis, 2003), compared to only 3.5-5.5 mmol/L in often used washing buffers or normal plasma. This preference of MSCs for the Ti-patterns over the Si-background has also been demonstrated in our previous study, using SEM for tracing of the cells (Myllymaa *et al*., 2010). In the current study ToF-SIMS was used to trace the cellular footprints, which first become visible after the removal of the cells. Metal ions (K^+) are not a quantitative indicator, since they could, in part, represent residuals from washing steps. However, they indicate a qualitative shift in their preferential binding after MSC culture and dominate the positive ion spectrum signal-noise when compared to the larger m/z cations.

Use of trypsin to remove cells and bacteria from the model surfaces could remove certain protein-based and trypsin-sensitive adherent fragments that were not analysed using the surface methods employed. This pre-treatment was anyway necessary, because in contrast to many previous cellular studies (which have focused on the cellular material on substrates), we focused on the ECM and EPS footprints left behind by eukaryotic and bacterial cells, respectively. The main point is that the footprints left by eukaryotic cells and bacterial cells were different, even though removal of cells by trypsin had caused some artefactual loss of the trypsin sensitive structures.

The substrate heavily influences the ion yields and fragmentation patterns detected by ToF-SIMS and therefore, fragment yields, ratios and efficiencies are likely to differ between DLC, titanium and various polymers or glasses. In spite of this, the footprint left by the eukaryotic cells and *Staphylococci* was different on all tested materials, suggesting that the footprints produced by the cells were specific to the type of cell which produced it. However, when the footprint produced by e.g., eukaryotic cells is compared between two or several different biomaterial substrates, the differences might be due to differences in the composition of the footprints, but might also in part reflect the dependence of the fragment yields on the different substrates, such as DLC or titanium.

Photolithography can leave residues on the surface, which cannot be detected by XPS but are detected by ToF-SIMS (Dubey *et al*., 2009), which may act as a confounding factor. Therefore, the results are not quantitative, but should be considered as a comparison between different systems. For example, in the present work different cells were tested using similarly treated cell culture substrate materials. Cell exposed samples were compared to media exposed samples, in which experiments both of the media used were studied. It was found that the footprints of *S. aureus* were rather similar on all the studied substrates and different from the footprints left by MSCs. This emphasises the potential of ToF-SIMS for the detection of implant-related infections caused by bacteria, even in cases that are already culture negative.

These results are preliminary and the study needs to be continued by comparing actual implants, which have been removed from patients. This research provides a new option for retrospective studies, even in bacterial culture negative cases, if the surface of clinical implants eventually shows footprints of bacteria or eukaryotic cells, a new approach worth examining.

Conclusions

In contrast to XPS, ToF-SIMS is a potential tool for the differentiation of bacterial from eukaryotic acellular footprints and may have potential in the *post-hoc* diagnosis of colonisation, biofilm formation and implant-related infections even in culture negative cases. Furthermore, ToF-SIMS analysis seems to be suitable for analysis of biocompatibility of different growth substrates, because the type and extent of the footprint indicates how the cells adhered and thrived on the implant surface provided for growth. ToF-SIMS can even be used to study protein adsorption indirectly, because the ToF-SIMS experiments also showed the 'race for the surface' phenomenon in protein binding. This was clearly influenced by the zeta-potential, both overall as well as exclusively for some components.

Acknowledgements

The authors acknowledge Helga Hildebrand for the ToF-SIMS and XPS and Anja Friedrich for SEM investigations (Univ. Erlangen-Nürenberg), Veikko Sariola (Univ. Helsinki) for helping with data analysis, Sami Myllymaa and Hannu Korhonen (Univ. Eastern Finland) for fabricating some samples, Montserrat Español Pons and Maria-Pau Ginebra (the Department of Materials Science and Metallurgy, Technical University of Catalonia, Barcelona, Spain) for help with the zeta-potential measurements and the Laboratory of Radiochemistry, Department of Chemistry, University of Helsinki for sterilising samples. We acknowledge the support of Finska Läkaresällskapet, the National Doctoral Programme of Musculoskeletal Disorders and Biomaterials, Helsinki University Central Hospital evo grants, ORTON Invalid Foundation, Individualised Musculoskeletal Medicine project of the Danish Council of Strategic Research and Regenerative Medicine RNP of the European Science Foundation.

References

Barnes CA, Brison J, Michel R, Brown BN, Castner DG, Badylak SF, Ratner BD (2011) The surface molecular functionality of decellularized extracellular matrices. Biomaterials **32**: 137-143.

Berbari EF, Marculescu C, Sia I, Lahr BD, Hanssen AD, Steckelberg JM, Gullerud R, Osmon DR (2007) Culture-negative prosthetic joint infection. Clin Infect Dis **45:** 1113-1119.

Bernsmann F, Lawrence N, Hannig M, Ziegler C, Gnaser H (2008) Protein films adsorbed on experimental dental materials: ToF-SIMS with multivariate data analysis. Anal Bioanal Chem **391**: 545-554.

Brown BN, Barnes CA, Kasick RT, Michel R, Gilbert TW, Beer-Stolz D, Castner DG, Ratner BD, Badylak SF (2010) Surface characterization of extracellular matrix scaffolds. Biomaterials **31**: 428-437.

Cai K, Frant M, Bossert J, Hildebrand G, Liefeith K, Jandt KD (2006) Surface functionalized titanium thin films: zeta-potential, protein adsorption and cell proliferation. Colloids Surf B Biointerfaces **50**: 1-8.

Canavan HE, Cheng X, Graham DJ, Ratner BD, Castner DG (2005a) Surface characterization of the extracellular matrix remaining after cell detachment from a thermoresponsive polymer. Langmuir **21**: 1949-1955.

Canavan HE, Cheng X, Graham DJ, Ratner BD, Castner DG (2005b) Cell sheet detachment affects the extracellular matrix: a surface science study comparing thermal liftoff, enzymatic, and mechanical methods. J Biomed Mater Res A **75**: 1-13.

Canavan HE, Cheng X, Graham DJ, Ratner BD, Castner DG (2006) A plasma-deposited surface for cell sheet engineering: advantages over mechanical dissociation of cells. Plasma Process. Polym. **3**: 516-523.

Canavan HE, Graham DJ, Cheng X, Ratner BD, Castner DG (2007) Comparison of native extracellular matrix with adsorbed protein films using secondary ion mass spectrometry. Langmuir **23**: 50-56.

Chatterjea A, Meijer G, van Blitterswijk C, de Boer J (2010). Clinical application of human mesenchymal stromal cells for bone tissue engineering. Stem Cells Int **11**: 215625.

Costerton JW, Stewart PS, Greenberg EP (1999) Bacterial biofilms: a common cause of persistent infections. Science **284**: 1318-1322.

Cunningham CD, Slattery HW, Luxford WM (2004) Postoperative infection in cochlear implant patients. Otolaryngol Head Neck Surg **131**: 109-114.

Darouiche RO (2001) Device-associated infections: a macroproblem that starts with microadherence. Clin Infect Dis 33: 1567-1572.

Darouiche RO (2004) Treatment of infections associated with surgical implants. N Engl J Med **350**: 1422-1429.

Donlan RM (2002) Biofilms: microbial life on surfaces. Emerging Infect Dis **8**: 881-890.

Dubey M, Emoto K, Cheng F, Gamble LJ, Takahashi H, Grainger DW, Castner DG (2009) Surface analysis of photolithographic patterns using ToF-SIMS and PCA. Surf Interface Anal **41**: 645-652.

Esquenazi E, Yang YL, Watrous J, Gerwick WH, Dorrestein PC (2009). Imaging mass spectrometry of natural products. Nat Prod Rep **26**: 1521-1534.

Gasper GL, Carlson R, Akhmetov A, Moore JF, Hanley L (2008) Laser desorption 7.87 eV postionization mass spectrometry of antibiotics in Staphylococcus epidermidis bacterial biofilms. Proteomics **8**: 3816-3821.

Girgis M (2003) Potassium and anaesthesia. Update Anaesth **17**: 1.

Ghosal S, Fallon SJ, Leighton TJ, Wheeler KE, Kristo MJ, Hutcheon ID, Weber PK (2008) Imaging and 3D elemental characterization of intact bacterial spores by high resolution secondary ion mass spectrometry. Anal Chem **80**: 5986-5992.

Goto T, Brunette DM (1998) Surface topography and serum concentration affect the appearance of tenascin in human gingival fibroblasts *in vitro*. Exp Cell Res **244**: 474-480.

Gristina AG (1987) Biomaterial-centered infection: microbial adhesion versus tissue integration. Science **237**: 1588-1595.

Gristina AG, Costerton JW (1985) Bacterial adherence to biomaterials and tissue. The significance of its role in clinical sepsis. J Bone Joint Surg Am **67**: 264-273.

Henry M, Bertrand P (2009) Surface composition of insulin and albumin adsorbed on polymer substrates as revealed by multivariate analysis of ToF-SIMS data. Surf Interface Anal **41**: 105-113.

Jungnickel H, Jones EA, Lockyer NP, Oliver SG, Stephens GM, Vickerman JC (2005) Application of TOF-SIMS with chemometrics to discriminate between four different yeast strains from the species Candida glabrata and Saccharomyces cerevisiae. Anal Chem **77**: 1740-1745.

Kaivosoja E, Barreto G, Levón K, Virtanen S, Ainola M, Konttinen YT (2011) Chemical and physical properties of regenerative medicine materials controlling stem cell fate. Ann Med, in press.

Killian MS, Krebs HM, Schmuki P (2011) Protein denaturation detected by time-of-flight secondary ion mass spectrometry. Langmuir **27**: 7510-7515.

Konttinen YT, Kaivosoja E, Stegaev V, Wagner HD, Levón J, Tiainen V-M, Mackiewicz Z (2011) Extracellular matrix and tissue regeneration. In: Steinhoff G (ed) Regenerative Medicine - from Protocol to Patient. Springer, London, pp 21-80.

Kulp KS, Berman ESF, Knize MG, Shattuck DL, Nelson EJ, Wu L, Montgomery JL, Felton JS, Wu KJ (2006) Chemical and biological differentiation of three human breast cancer cell types using time-of-flight secondary ion mass spectrometry. Anal Chem **78**: 3651-3658.

Levon J, Myllymaa K, Kouri V-P, Rautemaa R, Kinnari T, Myllymaa S, Konttinen YT, Lappalainen R (2010) Patterned macroarray plates in comparison of bacterial adhesion inhibition of tantalum, titanium, and chromium compared with diamond-like carbon. J Biomed Mater Res A **92**: 1606-1613.

Lhoest JB, Wagner MS, Tidwell CD, Castner DG (2001) Characterization of adsorbed protein films by time of flight secondary ion mass spectrometry. J Biomed Mater Res **57**: 432-440.

Marculescu CE, Berbari EF, Hanssen AD, Steckelberg JM, Osmon RD (2005) Prosthetic joint infection diagnosed postoperatively by intraoperative culture. Clin Orthop Relat Res **439**: 38-42.

Malekzadeh D, Osmon DR, Lahr BD, Hanssen AD, Berbari EF (2010) Prior use of antimicrobial therapy is a risk factor for culture-negative prosthetic joint infection. Clin Orthop Relat Res **468**: 2039-2045.

Mustafa K, Pan J, Wroblewski J, Leygraf C, Arvidson K (2002) Electrochemical impedance spectroscopy and x-ray photoelectron spectroscopy analysis of titanium surfaces cultured with osteoblast-like cells derived from human mandibular bone. J Biomed Mater Res **59**: 655-664.

Myllymaa K, Myllymaa S, Korhonen H, Tiitu V, Lammi M, Lappalainen R (2009) Interactions between SaOS-2 cells and microtextured amorphous diamond or amorphous diamond hybrid coated surfaces with different wettability properties. Diam Relat Mater **18**: 1294-1300.

Myllymaa S, Kaivosoja E, Myllymaa K, Sillat T, Korhonen H, Lappalainen R, Konttinen YT (2010) Adhesion, spreading and osteogenic differentiation of mesenchymal stem cells cultured on micropatterned amorphous diamond, titanium, tantalum and chromium coatings on silicon. J Mater Sci Mater Med **21**: 329-341.

Neut D, van Horn JR, van Kooten TG, van der Mei HC, Busscher HJ (2003) Detection of biomaterial-associated infections in orthopaedic joint implants. Clin Orthop Relat Res **413**: 261-268.

Page K, Wilson M, Parkin IP (2009) Antimicrobial surfaces and their potential in reducing the role of the inanimate environment in the incidence of hospital-acquired infections. J Mater Chem **19**: 3819-3831

Panousis K, Grigoris P, Butcher I, Rana B, Reilly JH, Hamblen DL (2005) Poor predictive value of broad-range PCR for the detection of arthroplasty infection in 92 cases. Acta Orthop **76**: 341-346.

Saldarriaga Fernández IC, Da Silva Domingues JF, van Kooten TG, Metzger S, Grainger DW, Busscher HJ, van der Mei HC (2011a) Macrophage response to staphylococcal biofilms on crosslinked poly(ethylene) glycol polymer coatings and common biomaterials *in vitro*. Eur Cell Mater **21**: 73-79.

Saldarriaga Fernández IC, Busscher HJ, Metzger SW, Grainger DW, van der Mei HC (2011b) Competitive time- and density-dependent adhesion of staphylococci and osteoblasts on crosslinked poly(ethylene glycol)-based polymer coatings in co-culture flow chambers. Biomaterials **32**: 979-984

Samuel NT, Wagner MS, Dornfeld KD, Castner DG (2001) Analysis of poly-amino acids by static time-of-flight secondary ion mass spectrometry TOF-SIMS. Surface Science Spectra **8**: 163-184.

Santavirta S, Gristina AG, Konttinen YT (1992) Cemented versus cementless hip arthroplasty. A review of prosthetic biocompatibility. Acta Orthop Scand **63**: 225-232.

Shin YN, Kim BS, Ahn HH, Lee JH, Kim KS, Lee JY, Kim MS, Khang G, Lee HB (2008) Adhesion comparison of human bone marrow stem cells on a gradient wettable surface prepared by corona treatment. Appl Surf Sci **255**: 293-296.

Sohail MR, Uslan DZ, Khan AH, Friedman PA, Hayes DL, Wilson WR, Steckelberg JM, Stoner S, Baddour LM (2007) Management and outcome of permanent pacemaker and implantable cardioverterdefibrillator infections. J Am Coll Cardiol **49**: 1851-1859.

Stevens JS, Schroeder SLM (2009) Quantitative analysis of saccharides by X-ray photoelectron spectroscopy. Surf Interface Anal **41**:453-462.

Trampuz A, Widmer AF (2006) Infections associated with orthopedic implants. Curr Opin Infect Dis **19**: 349-356.

Trampuz A, Zimmerli W (2006) Diagnosis and treatment of infections associated with fracture-fixation devices. Injury **37**:S59-S66.

Tunney MM, Patrick S, Curran MD, Ramage G, Hanna D, Nixon JR, Gorman SP, Davis RI, Anderson N (1999) Detection of prosthetic hip infection at revision arthroplasty by immunofluorescence microscopy and PCR amplification of the bacterial 16S rRNA gene. J Clin Microbiol **37**: 3281-3290.

Tyler BJ, Rangaranjan S, Möller J, Beumer A, Arlinghaus HF (2006) TOF-SIMS imaging of chlorhexidine-digluconate transport in frozen hydrated biofilms of the fungus Candida albicans. Appl Surf Sci **252**: 6712-6715.

Valle J, Toledo-Arana A, Berasain C, Ghigo JM, Amorena B, Penades JR, Lasa I (2003) SarA and not sigmaB is essential for biofilm development by Staphylococcus aureus. Mol Microbiol **48**: 1075-1087.

Wagner MS, Castner DG (2001) Characterization of adsorbed protein films by time-of-flight secondary ion mass spectrometry with principal component analysis. Langmuir **17**: 4649-4660.

Wagner MS, McArthur SL, Shen M, Horbett TA, Castner DG (2002a) Limits of detection for time of flight secondary ion mass spectrometry (ToF-SIMS) and X-ray photoelectron spectroscopy (XPS): detection of low amounts of adsorbed protein. J Biomater Sci Polym Ed **13**: 407-428.

Wagner MS, Tyler BJ, Castner DG (2002b) Interpretation of static time-of-flight secondary ion mass spectra of adsorbed protein films by multivariate pattern recognition. Anal Chem **74**: 1824-1835.

Wagner MS, Horbett TA, Castner DG (2003a) Characterizing multicomponent adsorbed protein films using electron spectroscopy for chemical analysis, time-of-flight secondary ion mass spectrometry, and radiolabeling: capabilities and limitations. Biomaterials **24**: 1897-1908.

Wagner MS, Shen M, Horbett TA, Castner DG (2003b) Quantitative analysis of binary adsorbed protein films by time of flight secondary ion mass spectrometry. J Biomed Mater Res A **64**: 1-11.

Xia N, May CJ, McArthur SL, Castner DG (2002) Time-of-flight secondary ion mass spectrometry analysis of conformational changes in adsorbed protein films. Langmuir **18**: 4090-4097.

Zimmerli W (2006) Infection and musculoskeletal conditions: Prosthetic-joint-associated infections. Best Pract Res Clin Rheumatol **20**: 1045-1063.

Discussion with Reviewers

Reviewer I: Can you give some ideas how to solve/treat this problems/diagnosis which are more present today than for 30 years ago?
Authors: To be able to create better implants and biomaterials it is critical to understand the reasons for failure. ToF-SIMS may provide less false negative and false positive results than currently used methods to detect implant-related deep infections and could thus provide accurate information even in antibiotic treated cases. Secondly, this approach could be used for *in vitro* testing of new implant coatings to indicate how well they are able to resist bacterial adhesion and production of extracellular polymeric matrix (biofilm, bacterial slime).

Reviewer II: What is your opinion about the practicality of doing such an analysis routinely, i.e. are these expensive pieces of equipment requiring specialists to use them?
Authors: When the differences between footprints of the host cells and bacteria have been clarified, specific components of the footprint might be identified with other less expensive methods, even in routine clinical use. We believe that, at present, this technique is most relevant for research and development of new biomaterials and coatings and is too expensive for routine clinical use.

At least some cases of failed orthopaedic implants that were considered aseptic loosening, based on the absence of clinical signs of infection and the failure to isolate bacteria, may actually have an infectious etiology (Nelson *et al*., 2005, additional reference). The footprint analysis, done after the removal of the implant and demonstrating bacterial footprints, could then suggest septic loosening in retrospect, even in culture negative cases. This could have also clinical relevance for the follow-up of the revision operated patient, because a full clearance of the infection is considered to be important in the prevention of recurrent infections and such patients might have an increased risk of such a recurrence (Engelsman *et al*., 2010, additional reference). In particular, the exact reason for the implant failure is crucial for researchers and developers, who try to evaluate the true incidence of infections and to develop new biomaterials and coatings able to resist bacterial adherence and biofilm formation. Only by understanding the reasons of implant failures will we be able to create better implants in the future.

In addition, the analysis is relatively fast to perform. Of course, this technique, due to the relatively small size of the sample chamber, is not at present suitable for large-size implants, such as hip implants, but would be perfect for small implants, such as middle ear implants.

Reviewer II: Do you expect that this same technique will be able to detect other microorganisms, such as *Staphylococcus epidermidis*, *Pseudomonas aeruginosa* etc? Furthermore, do you expect that it would work in the presence of different types of eukaryotic cells such as osteoblasts, fibroblasts etc.?
Authors: We would expect that by using similar amino acid based segmentation, biofilm producing bacteria can be separated from eukaryotic cells, even if there are multiple different types of eukaryotic cells present. It could be even possible to detect the type of the micro-organism and cells, although that can be challenging from the footprint only.

Reviewer II: Why not select secreted protein peaks known to be unique to prokaryotes *versus* eukaryotes and use these as a basis for imaging contrast?
Authors: This could be an interesting approach. However, proteins that are adsorbed on the surface do not represent exactly the composition of proteins in the bulk solution. Generally speaking, the proteins that have the greatest mobility are adsorbed first and are later replaced by proteins that have a higher affinity for surface. Protein-surface interactions result in high local concentrations of the protein, reaching concentrations up to 1000 times higher than in the bulk solution. Respectively, some proteins strongly expressed in the bulk solution, might not be present at the surface at all. Therefore, components, which in the preliminary analysis of the ToF-SIMS spectra showed difference between MSC and *S. aureus* samples, were selected for imaging.

Reviewer II: What influence does co-culture medium have on the matrix production of each cell type?
Authors: The co-culture media did not influence the amount of EPS production by *S. aureus*. However, co-culture stress could lead to stressed phenotypes of the cultured cells and deposition of stress-related matrix proteins on the surface of the culture substrate, which could affect cellular adhesion.

Reviewer II: Is linear subtraction of ToF-SIMS peak sets appropriate, given their non-linear intensity correlations from many different matrix effects specific to each ion fragment?
Authors: With the background subtraction we used, it was possible to reduce the effect of the different media used (MSCGM or TSB). Peaks that can originate from several different amino acids (marked with a star in Table 1) were not included in the analysis and therefore, linear subtraction is a relatively good approximation. However, in general, the relationship of the background to the ToF-SIMS peaks is far from simple and some more sophisticated method could give a better approximation for the background. Nonetheless, even when we tested the separation of MSC samples and co-culture samples (both cultured in MSCGM) without any subtraction, it was possible to separate the samples.

Additional References

Engelsman AF, Saldarriaga-Fernandez IC, Nejadnik MR, van Dam GM, Francis KP, Ploeg RJ, Busscher HJ, van der Mei HC (2010) The risk of biomaterial-associated infection after revision surgery due to an experimental primary implant infection. Biofouling **26**: 761-767.

Nelson CL, McLaren AC, McLaren SG, Johnson JW, Smeltzer MS (2005) Is aseptic loosening truly aseptic? Clin Orthop Relat Res **437**: 25-30.